J|A|C|S
ARTICLES
Published on Web 04/06/2004

Multinuclear NMR Investigations of the Oxygen, Water, and Hydroxyl Environments in Sodium Hexaniobate

Todd M. Alam,*,† May Nyman,‡ Brian R. Cherry,† Judith M. Segall,† and Leslie E. Lybarger‡

Contribution from the Department of Organic Materials and Department of Geochemistry, Sandia National Laboratories, Albuquerque, New Mexico 87185

Received November 26, 2003; E-mail: tmalam@sandia.gov

Abstract: Solid-state ^{1}H, ^{17}O MAS NMR, $^{1}H-^{93}Nb$ TRAPDOR NMR, and ^{1}H double quantum 2D MAS NMR experiments were used to characterize the oxygen, water, and hydroxyl environments in the monoprotonated hexaniobate material, $Na_7[HNb_6O_{19}]\cdot 15H_2O$. These solid-state NMR experiments demonstrate that the proton is located on the bridging oxygen of the $[Nb_6O_{19}]^{8-}$ cluster. The solid-state NMR results also show that the NbOH protons are spatially isolated from similar protons, but undergo proton exchange with the water species located in the crystal lattice. On the basis of double quantum ^{1}H MAS NMR measurements, it was determined that the water species in the crystal lattice have restricted motional dynamics. Two-dimensional $^{1}H-^{17}O$ MAS NMR correlation experiments show that these restricted waters are preferentially associated with the bridging oxygen. Solution ^{17}O NMR experiments show that the hydroxyl proton is also attached to the bridging oxygen for the compound in solution. In addition, solution ^{17}O NMR kinetic studies for the hexaniobate allowed the measurement of relative oxygen exchange rates between the bridging, terminal, and hydroxyl oxygen and the oxygen of the solvent as a function of pH and temperature. These NMR experiments are some of the first investigations into the proton location, oxygen and proton exchange processes, and water dynamics for a base stable polyoxoniobate material, and they provide insight into the chemistry and reactivity of these materials.

Introduction

The Lindquist ion, $[Nb_6O_{19}]$,$^{8-}$ also known as hexaniobate, is the cornerstone of polyoxoniobate chemistry. It is the dominant species of basic (pH > 7) niobium oxide solutions[1,2] and is one of the few polyoxoniobate structures that have been characterized in the solid state. The solid-state structure of a hexaniobate salt was first reported in 1980 as a 7/6 salt; meaning seven charge-balancing sodiums and six NbO_6 octahedra in the cluster.[3] Other solid-state polyoxoniobate structures include the decaniobate $[Nb_{10}O_{28}]^{6-}$ cluster,[4] a material featuring chains of the Keggin ion,[5] $[SiNb_{12}O_{40}]$,$^{16-}$ and a new heteropolyanion geometry composed of 16 NbO_6 octahedra and 2 SiO_4 tetrahedra with a central Si_2O_7 unit.[5] In our ongoing investigations on synthesis, stability, and reactivity of polyoxoniobates, we have observed that hexaniobate can be used as a precursor for synthesis of other polyoxoniobates and that the hexaniobate cluster is sometimes an intermediate product to the formation of other polyoxoniobate geometries. Additionally, several synthetic and structural studies have shown that hexaniobate can behave as an anionic ligand and coordinate metals including Mn(IV) and Ni(IV),[6,7] Mn(I) and Re(I),[8] and Al(III) and Eu(III).[9]

It is likely that protons play an important role in the metal binding process as well as the stability of the Lindquist ion in solution. One study suggested that the degree of protonation of the $[Nb_6O_{19}]^{8-}$ cluster in solution is pH-dependent and ranges from zero to three per cluster unit and decreases with increasing pH between $8.5 < pH < 11.5$.[10] Protons and metals are predicted to coordinate to the most basic site within the cluster. The nature of protonation of polyoxometalates is key to metal coordination in the solid state since the coordination mechanism may involve replacement of protons with metals. The coordination of Mn, Ni, Re, and Al to the hexaniobate cluster in their respective complexes is similar; the metal binds to bridging oxygens of edge-sharing NbO_6 octahedra.[6−9] In contrast, Eu coordinates both bridging and terminal oxygens in the hexaniobate cluster.[9] The solution stability of polyoxoniobates is also dependent on the proton binding to the anionic cluster, with increased binding and lower complex stability at lower pH values. To date,

† Department of Organic Materials.
‡ Department of Geochemistry.

(1) Rozantsev, G. M.; Dotsenko, O. I.; Taradina, G. V. *Russ. J. Coord. Chem.* **2000**, *26*, 247.
(2) Muller, M. *Rev. Chim. Miner.* **1970**, *7*, 359−411.
(3) Goiffon, A.; Philippot, E.; Maurin, M. *Rev. Chim. Miner.* **1980**, *17*, 466−476.
(4) Graeber, E. J.; Morosin, B. *Acta Crystallogr.* **1977**, *B33*, 2137−2143.
(5) Nyman, M.; Bonhomme, F.; Alam, T. M.; Rodriguez, M. A.; Cherry, B. R.; Krumhansl, J. L.; Nenoff, T. M.; Sattler, A. M. *Science* **2002**, *297*, 996−998.
(6) Flynn, C. M.; Stucky, G. D. *Inorg. Chem.* **1969**, *8*, 332−334.
(7) Flynn, C. M.; Stucky, G. D. *Inorg. Chem.* **1969**, *8*, 335−344.
(8) Besserguenev, A. V.; Dickman, M. H.; Pope, M. T. *Inorg. Chem.* **2001**, *40*, 2582−2586.
(9) Ozeki, T.; Yamase, T.; Naruke, H.; Sasaki, Y. *Bull. Chem. Soc. Jpn.* **1994**, *67*.
(10) Goiffon, A.; Granger, R.; Bockel, C.; Spinner, B. *Rev. Chim. Miner.* **1973**, *10*, 487−502.

10.1021/ja0398159 CCC: $27.50

literature on the location and behavior of protons in $[H_xNb_6O_{19}]^{8-x}$ ($x = 0-3$) materials, both in solution and in the solid state, is conflicting. For example, the structure reported by Goiffon et al.[3] for the monohydrogen heptasodium hexaniobate material, $Na_7(H_3O^+)[Nb_6O_{19}]\cdot 14H_2O$, describes a H_3O^+ within bonding distance of a bridging oxygen, but the authors interpreted the structural data as the proton of H_3O^+ being mainly associated with the water molecule. In contrast, Muller[2] deduced from the solid-state IR and Raman spectroscopy data that the proton is associated with a terminal oxygen of the $[Nb_6O_{19}]^{8-}$ for the monoprotonated hexaniobate and associated with both the terminal and bridging oxygens in the diprotonated cluster. On the other hand, Ozeki and co-workers[9] determined by X-ray diffraction the location of the protons for the diprotonated hexaniobate hydrate, $Na_6[H_2Nb_6O_{19}]\cdot 20H_2O$, to be only on the bridging oxygen sites of the cluster.

A variety of multinuclear NMR experiments have been utilized (including ^{17}O, ^{1}H, ^{31}P, ^{51}V) to investigate the role of protons in catalytically active polyoxometalates.[11−27] The majority of the solid-state ^{1}H magic angle spinning (MAS) NMR studies have focused on dehydrated forms of the Keggin anions. Investigations into the effect of H_2O in the crystal lattice on protonation of polyoxometalates materials are rare. Solution ^{17}O NMR has been used to identify the protonation site in the polyoxometalate complexes.[22,23,28−31] Comparison of the ^{17}O NMR chemical shift between solution and solid-state NMR spectra was also used to identify the protonation site in $H_3PW_{12}O_{40}$.[24,25] More recently, a series of rotational echo double resonance NMR experiments have shown the proton location to be on the bridging oxygen position in $H_3PMo_{12}O_{40}$, while the proton is located on the terminal oxygen position for $H_3PW_{12}O_{40}$.[32]

From these previous investigations, the location and nature of the proton sites in polyoxometalates (predominantly polyoxotungstates and polyoxomolybdates) and the differences between the crystalline solid-state structure and the solution structure appear to be highly variable. No previous NMR studies have addressed the proton location in polyoxoniobates. Details concerning the water and oxygen environments in polyoxoniobates are also lacking. We expect the behavior of the polyoxoniobates in aqueous solution to be much different than that of the better-studied polyoxotungstates and polyoxomolybdates, since the latter are stable in acidic solutions and the niobates are stable in basic solutions. Furthermore, the niobates carry larger charge-to-surface ratios than the structurally similar tungstates and molybdates, which should also influence behavior in solution. In this article, we have used a series of multinuclear NMR techniques to gain a better understanding of the proton and oxygen environments and dynamics for the monoprotonated sodium hexaniobate in both the solid state and solution.

Experimental Section

Materials. (1) Synthesis of $Na_7[HNb_6O_{19}]\cdot 15H_2O$ (I). Sodium hydroxide (2.0 g, 50 mmol) was dissolved in ~1000 mL of deionized water, and the solution was heated to ~90 °C. While the solution was stirred, a total of 2.0 g of hydrous, amorphous Nb_2O_5 (10.5 mmol Nb; Reference Metals, Bridgeville, PA) was added by 0.2-g aliquots. Each aliquot was completely dissolved before the next aliquot was added. Following dissolution of all the Nb_2O_5, the solution was allowed to cool. After sitting 1−3 days at room temperature, colorless crystals deposited on the wall and bottom of the beaker. Approximately 2 g (1.5 mmol, 9.0 mmol Nb) of the crystals were collected by filtration. The product was identified as $H_3O\cdot Na_7[Nb_6O_{19}]\cdot 14H_2O$ by powder X-ray diffraction (JCPDF 84-0188). The yield was ~86% based on Nb.

(2) Synthesis of ^{17}O-Labeled $Na_7[HNb_6O_{19}]\cdot 15H_2O$. NaOH (0.28 g, 7.0 mmol) was dissolved in 1.2 g (63 mmol) of 40.2 atom % ^{17}O water (Isotec, Inc., Miamisburg, Ohio) in a 23-mL Teflon cup for a stainless steel autoclave. To this solution, 0.5 g of niobium (V) ethoxide (1.57 mmol $Nb(OC_2H_5)_5$, Aldrich) was added and stirred for 20 min. Hydrolysis and condensation of the $Nb(OC_2H_5)_5$ produced a white precipitate of hydrous niobium oxide that contained ~36 atom % ^{17}O, slightly diluted from the original 40.2% by the unlabeled NaOH. This labeled precursor mixture was then autoclaved at 190 °C for 1 h. The white powder product was collected by filtration and rinsed very minimally with unlabeled, deionized water. The product was collected (0.29 g, yield ~85% based on Nb) and identified as hexaniobate by powder X-ray diffraction (JCPDF 84-0188).

Solid-State NMR Spectroscopy. All of the solid-state ^{1}H MAS NMR experiments were performed on a Bruker Avance 600 operating at 600.14 MHz. Spectra were obtained using a 2.5-mm double resonance probe spinning between 30 and 35 kHz, with a 3-μs $\pi/2$ pulse length, 16−32 scan averages, 4-s recycle delay, nominally at 25 °C. The high spinning frequency caused additional heating of the sample, and from separate studies with $PbNO_3$ it was known that for 30 kHz spinning speeds the unregulated sample temperature was ~45 °C. The ^{1}H NMR chemical shifts were referenced to a H_2O secondary standard, $\delta = +4.8$ ppm, with respect to tetramethylsilane $\delta = 0.0$ ppm.

The 2D double quantum (DQ) correlation experiment and the 1D double quantum filtered (DQF) experiments utilized the chemical shift anisotropy (CSA) and offset compensated back-to-back (BABA)[33,34] multiple pulse train for the excitation and reconversion of multiple quantum coherences. For the 2D exchange experiment, the $0 \rightarrow \pm 2 \rightarrow 0 \rightarrow 1$ coherence pathway was selected using a 64 step phase cycle and used 128 rotor-synchronized t_1 increments, 3-μs $\pi/2$ pulses, an

(11) *NMR Techniques in Catalysis*; Bell, A. T., Pines, A., Eds.; Marcel Dekker: New York, 1994.
(12) Nakata, S.; Tanaka, Y.; Asaoka, S.; Nakamuram, M. *J. Mol. Struct.* **1998**, *441*, 267−281.
(13) *Solid-State NMR Spectrscopy of Inorganic Materials*; Fitzgerald, J. J., Ed.; American Chemical Society: Washington, DC, 1999; Vol. 117.
(14) Baba, T.; Ono, K. Y. In *Annual Reports on NMR Spectroscopy*; Webb, G. A., Ed.; Academic Press: San Diego, CA, 1999; Vol. 38, pp 356−390.
(15) English, A. D.; Jesson, J. P.; Klemperer, W. G.; Mamouneas, T.; Messerle, L.; Shum, W.; Tramontano, A. *J. Am. Chem. Soc.* **1975**, *97*, 4785−4786.
(16) Filowitz, M.; Klemperer, W. G.; Messerle, L.; Shum, W. *J. Am. Chem. Soc.* **1976**, *98*, 2345−2346.
(17) Klemperer, W. G. *Angew. Chem., Int. Ed. Engl.* **1978**, *17*, 246−254.
(18) Filowitz, M.; Ho, R. K. C.; Klemperer, W. G.; Shum, W. *Inorg. Chem.* **1979**, *18*, 93−103.
(19) Besecker, C. J.; Klemperer, W. G.; Maltbie, D. J.; Wright, D. A. *Inorg. Chem.* **1985**, *24*, 1027−1032.
(20) Damyanova, S.; Fierro, J. L. G.; Sobrados, I.; Sanz, J. *Langmuir* **1999**, *15*, 469−476.
(21) Huang, W.; Todaro, L.; Francesconi, L. C.; Polenova, T. *J. Am. Chem. Soc.* **2003**, *125*, 5928−5938.
(22) Klemperer, W. G.; Shum, W. *J. Am. Chem. Soc.* **1977**, *99*, 3544−3545.
(23) Klemperer, W. G.; Shum, W. *J. Am. Chem. Soc.* **1978**, *100*, 4891−4893.
(24) Kozhevnikov, I. V.; Sinnema, A.; Jansen, R. J. J.; van Bekkum, H. *Mendeleev Commun.* **1994**, *4*, 92−93.
(25) Kozhevnikov, I. V.; Sinnema, A.; Jansen, R. J. J.; van Bekkum, H. *Catal. Lett.* **1994**, *27*, 187−197.
(26) Duncan, D. C.; Hill, C. L. *Inorg. Chem.* **1996**, *35*, 5828−5835.
(27) Kozhevnikov, I. V.; Sinnema, A.; van Bekkum, H.; Fournier, M. *Catal. Lett.* **1996**, *41*, 153−157.
(28) Pohl, M.; Lyon, D. K.; Mizuno, N.; Nomiya, K.; Finke, R. G. *Inorg. Chem.* **1995**, *34*, 1413−1429.
(29) Klemperer, W. G.; Main, D. J. *Inorg. Chem.* **1990**, *29*, 2355−2360.
(30) Day, V. W.; Klemperer, W. G.; Main, D. J. *Inorg. Chem.* **1990**, *29*, 2345−2355.
(31) Day, V. W.; Klemperer, W. G.; Schwartz, C. *J. Am. Chem. Soc.* **1987**, *109*, 6030−6044.
(32) Ganapathy, S.; Fournier, M.; Paul, J. F.; Delevoye, L.; Guelton, M.; Amoureux, J. P. *J. Am. Chem. Soc.* **2002**, *124*, 7821−7828.
(33) Feike, M.; Demco, D. E.; Graf, R.; Gottwald, J.; Hafner, S.; Spiess, H. W. *J. Magn. Reson., Ser. A* **1996**, *122*, 214−221.
(34) Schnell, I.; Spiess, H. W. *J. Magn. Reson.* **2001**, *151*, 153−227.

excitation−reconversion length of $\tau_{exc} = 66.66$ μs, and a dephasing delay of 33.33 μs. For these excitation times, the observation of a signal in the DQ spectra implied the existence of dipolar coupling between a pair of nuclei with ^{1}H−^{1}H distances <3.5Å.

The ^{1}H−^{93}Nb transfer of population in double resonance (TRAPDOR) NMR experiments used a rotor-synchronized ^{1}H spin−echo, during which the quadrupolar ^{93}Nb spins were irradiated during the evolution period. The TRAPDOR fraction $[(S_0 - S)/S_0]$ was obtained by subtracting the TRAPDOR spectra (S) from the control spectra (S_0) for which there was no ^{93}Nb irradiation during the spin−echo. A detailed description of these TRAPDOR NMR experiments has previously been given.[35−37] The ^{1}H−^{93}Nb TRAPDOR NMR experiments were obtained using 128 scan averages, 4-s recycle delays, spinning speeds ranging from 20 to 30 kHz, evolution periods from 1 to 8 rotor cycles, and a ^{93}Nb irradiation field of 62.5 kHz at a ^{93}Nb resonant frequency of 146.73 MHz. The magnitude of the TRAPDOR fraction is a function of the dipolar coupling constant and the adiabaticity parameter (α) proposed by Grey and co-workers.[35−37] The value of α is a function of the quadrupolar coupling constant (ω_Q), the spinning speed (ω_R), and the irradiating field strength (ω_1) and is given by $\alpha = \omega_1^2/\omega_R\omega_Q$. It was noted that the ^{1}H−^{93}Nb TRAPDOR fraction obtained for compound **I** decreased with increased spinning speed or a decrease in the Nb rf power, suggesting that these ^{1}H−^{93}Nb experiments were not performed under the pure adiabatic transfer condition ($\alpha \gg 1$).

The solid-state ^{17}O NMR MAS spectra were obtained on both a Bruker Avance 600 instrument using an observe frequency of 81.40 MHz and a Bruker Avance 400 instrument with an observe frequency of 54.28 MHz. For the 81.40 MHz data the ^{17}O MAS NMR spectra were obtained using a 2.5-mm broadband probe with spinning speeds between 30 and 35 kHz, with 2-μs $\pi/6$ pulses ($\pi/2$ pulse length 6 μs), 1 K scan averages, and 5-s recycle delay. For the 54.28 MHz ^{17}O MAS NMR data and the ^{1}H−^{17}O cross-polarization (CP) MAS NMR data, a 4-mm broadband MAS probe spinning between 12.5 and 15 kHz was used. For all ^{17}O MAS NMR spectra high power ^{1}H decoupling was employed using the two-pulse phase modulation (TPPM) decoupling sequence.[38] The ^{1}H−^{17}O CPMAS NMR data was obtained using a 62.5 kHz ^{1}H field and a 20.83 kHz ^{17}O field, in agreement with the predicted matching condition for quadrupolar ^{17}O nuclei, $\omega_1(^1\text{H})/\omega_1(^{17}\text{O}) \approx 3$.[39] The 2D ^{1}H−^{17}O correlation experiments were performed using 4 K scan averages, 64 t_1 increments with a 125 kHz t_1 spectral window, 100 μs contact time, and TPPI phase-sensitive detection.

The solution ^{17}O NMR data were obtained on a Bruker Avance 600 instrument, operating at 81.40 MHz, using a 5-mm broadband probe. Direct Bloch decay spectra were obtained using standard sequences with 0.5-s recycle delay, 8-μs $\pi/2$ pulses, 512 scan averages, and ^{1}H decoupling. The ^{17}O NMR spectra were all referenced to external neat H_2O ($\delta = 0.0$ ppm) at 25 °C. For all solution ^{17}O NMR kinetic studies, 5 mg of the ^{17}O-labeled hexaniobate material was dissolved in 750 μL of water.

Simulation of DQ NMR Sideband Spectra. The signal intensity of these DQ sidebands (I_{DQ}) can be described by

$$I_{DQ}(t_1; t_2 = 0) = \cos(2\Delta\omega_{PC}t_1)\left\langle \sin\left[\frac{3}{\pi\sqrt{2}} D_{eff}^{ij} \sin(2\beta^{ij}) \cos(\gamma^{ij} + \omega_R t_1)N\tau_R\right] \times \sin\left[\frac{3}{\pi\sqrt{2}} D_{eff}^{ij} \sin(2\beta^{ij}) \cos(\gamma^{ij})N\tau_R\right]\right\rangle \quad (1)$$

where D_{eff}^{ij} is the effective dipolar coupling constant between nuclei i and j, $\Delta\omega_{PC}$ is the frequency increment for TPPI, t_1 is the evolution time step, ω_R is the MAS spinning frequency, N is the number of rotor periods in the excitation−reconversion component of the sequence, τ_R is the rotor period, β^{ij} and γ^{ij} are the Euler angles describing the orientation of the principal axis of the dipolar-coupling tensor between spins i and j in the reference frame fixed to the rotor, and the symbol $\langle\ \rangle$ represents the powder average.[40] Our lab has recently shown that in some situations a distribution of effective dipolar couplings greatly improves the simulated fit to the observed DQ spinning sideband pattern.[41] For the simulations presented, a Gaussian distribution of D_{eff}^{ij} is assumed. Details of the effect distributions have on the observed DQ spectra are given elsewhere.[41] The dipolar coupling (D^{ij}) between protons separated by a distance r_{ij} is given by

$$D^{ij} = -\frac{\mu_0 \hbar \gamma_i \gamma_j}{4\pi r_{ij}^3} \quad (2)$$

where μ_0 is the vacuum permeability and $\gamma_{i,j}$ is the magnetogyric ratios of the interacting protons.[34]

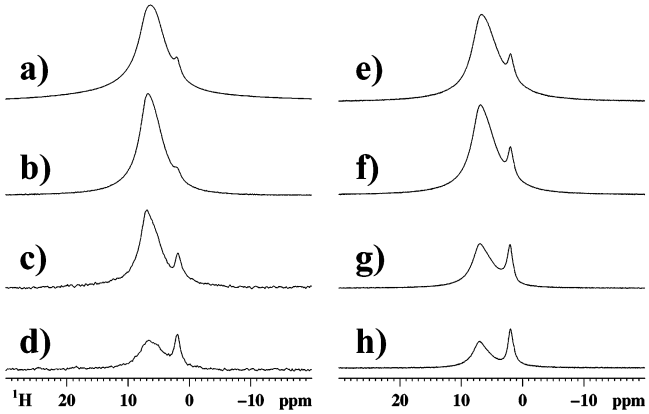

Figure 1. (a) 1D ^{1}H MAS NMR spectrum of (**I**) acquired using a single pulse direct Bloch decay. The DQF ^{1}H MAS NMR spectra with increasing excitation times: (b) τ_r (33 us), (c) $2\tau_r$ (66 us), and (d) $4\tau_r$ (132 us). The rotor-synchronized Hahn echo 1D ^{1}H MAS NMR spectra with different interpulse delays: (e) τ_r (33 μs), (f) $2\tau_r$ (66 μs), (g) $4\tau_r$ (132 μs), and (h) $6\tau_r$ (198 μs), where τ_r (= $1/\nu_r$) is the rotor period for given spinning frequency.

Results

The characterization of the oxygen, hydroxyl, and water environments in the sodium hexaniobate compound is described in this section. A variety of NMR methods were utilized to assign the observed ^{1}H and ^{17}O chemical shifts, plus provide a measure of the dipolar interactions and connectivities between different nuclei.

Fast Solid-State ^{1}H MAS NMR. The 1D ^{1}H MAS NMR spectra for compound (**I**) obtained at 33 kHz is shown in Figure 1a. Two proton resonances are observed: a broad signal (fwhm = 3160 Hz) at $\delta = +6.3$ ppm and a smaller narrow resonance (fwhm = 700 Hz) at $\delta = +1.9$ ppm. It was observed that at spinning speeds below ~20 kHz these two resonances become more difficult to resolve, probably a result of increased residual dipolar interactions. Even at these high spinning speeds multiple spinning sidebands are observed for the dominant broad resonance ($\delta = +6.3$ ppm), a demonstration of significant proton dipolar coupling for this proton species (see Figure 1S, Supporting Information). The variation of the ^{1}H NMR chemical

(35) Grey, C. P.; Vega, A. J. *J. Am. Chem. Soc.* **1995**, *117*, 8232−8242.
(36) Grey, C. P.; Eijkelenboom, A. P. A. M.; Veeman, W. *Solid State Nucl. Magn. Reson.* **1995**, *4*, 113−120.
(37) Grey, C. P.; Veeman, W. *Chem. Phys. Lett.* **1992**, *192*, 379−385.
(38) Bennet, A. E.; Rienstra, C. M.; Auger, M.; Lakshmi, K. V.; Griffin, R. G. *J. Chem. Phys.* **1995**, *103*, 6951−6958.
(39) Walter, T. H.; Turner, G. L.; Oldfield, E. *J. Magn. Reson.* **1988**, *76*, 106−120.
(40) Graf, R.; Demco, D. E.; Gottwald, J.; Hafner, S.; Spiess, H. W. *J. Chem. Phys.* **1997**, *106*, 885−895.
(41) Holland, G. P.; Cherry, B. R.; Alam, T. M. *J. Magn. Reson.* **2004**, *167*, 161−167.

shift for the $\delta \approx +1.9$ ppm resonance as a function of temperature is small, while the broad resonance at $\delta \approx +6.3$ ppm shows a variation of ~0.7 ppm between −13 and 52 °C. A summary of these VT results is included in the Supporting Information (Figure 2S). These variations of ^{1}H chemical shift during regulated VT control also demonstrate that the unregulated RT spectra actually correlate to a sample temperature of ~45 °C due to heating during high-speed spinning. The observed line widths for both resonances increased with higher temperatures (Figure 3S in Supporting Information), suggesting that both of the protons resonances are broadened due to a chemical exchange processes. The relative integration of the ^{1}H intensity (including integration of the entire spinning sideband manifold) of the $\delta = +1.9$ ppm resonance to the $\delta = +6.3$ ppm resonance was 1:29.5.

To further assist in the assignment of these ^{1}H MAS resonances, a series of DQF and rotor-synchronized spin−spin relaxation (T_2-filtered) Hahn echo ^{1}H MAS NMR spectra are shown in Figure 1. In Figure 1b−d, the broad resonance at +6.3 ppm is suppressed by the DQF in comparison to the narrower resonance at +1.9 ppm. A similar suppression of the broad +6.3 ppm resonance is observed in the T_2-filtered experiments shown in Figure 1e−h. The T_2 for the +6.3 ppm and the +1.9 ppm resonances at 30 kHz spinning were found to be 128 μs and 410 μs, respectively. These T_2 values are consistent for protons adsorbed/bound to zeolites. There is a small variation of T_2 as a function of spinning speed between 20 and 33 kHz (Figure 4S in Supporting Information), with the $\delta = +1.9$ ppm resonance showing the largest increase in T_2 (ranging from 300 to 400 μs) with increased sample spinning speed. It was difficult to accurately measure T_2 at slower spinning speeds (<20 kHz) due to decreased spectral resolution.

Solid-State 2D DQ ^{1}H MAS NMR Exchange Experiments. The 2D DQ ^{1}H MAS NMR exchange experiment for compound (**I**) obtained using a BABA excitation−reconversion sequence is shown in Figure 2. The DQ ^{1}H MAS NMR exchange spectra consist of the single-quantum (SQ) dimension (horizontal) plotted versus the DQ dimension (vertical), where dipolar interactions between different protons are observed as distinct resonances. Resonances that occur along the diagonal (ω, 2ω) are referred to as autocorrelation peaks and result from the dipolar interaction of protons with the same chemical shift. Off-diagonal resonances, (ω_a, $\omega_a + \omega_b$) and (ω_b, $\omega_a + \omega_b$), are produced from dipolar interactions between protons with different chemical shifts. For the short mixing times used in these 2D ^{1}H DQ NMR exchange experiments, the observation of a DQ signal implies that a dipolar coupling between protons that have separations <3.5 Å is occurring in compound (**I**). The lack of a DQ correlation results from the presence of only very long ^{1}H−^{1}H distances (weak dipolar couplings), a reduction (averaging) of the dipolar coupling due to rapid molecular motions, or from interference effects of molecular motions that are on the order of the NMR experiments (~100 μs). The 2D DQ ^{1}H MAS NMR spectrum for compound (**I**) shows a strong autocorrelation peak for the water resonance ($\delta = +6.3$ ppm) due to both intra- and intermolecular dipolar interactions between the two protons in water. There is no autocorrelation resonance observed in the 2D DQ ^{1}H MAS NMR exchange spectra for the resonance at $\delta = +1.9$ ppm, but a weak correlation resonance with the broad water resonance ($\delta = +6.3$ ppm) is observed.

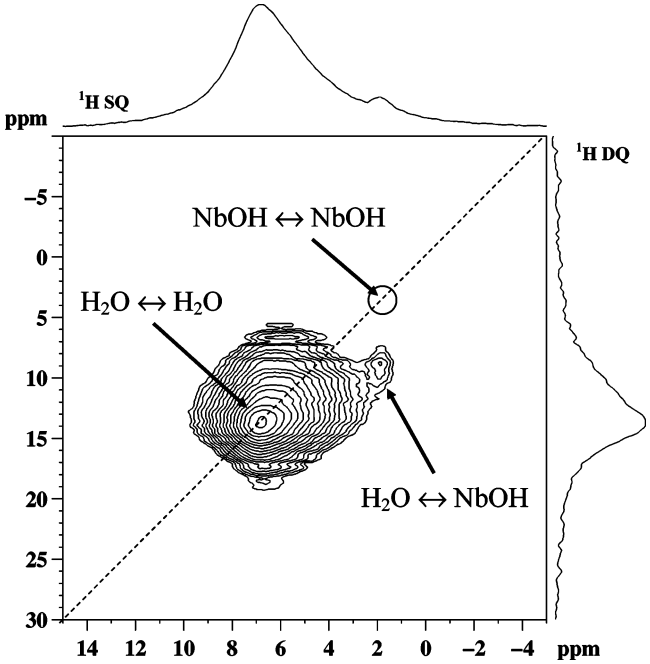

Figure 2. 2D DQ ^{1}H MAS NMR exchange spectra for compound (**I**) recorded at a spinning speed of 30 kHz using the BABA recoupling sequence with an excitation time of 66.66 μs. The SQ and DQ projections are shown on the top and right, respectively. The strong autocorrelation resonance for the broad adsorbed H_2O resonance ($\delta = +6.3$ ppm), the weak correlation between the different H_2O and NbOH proton species, along with the missing autocorrelation resonance for the NbOH resonance ($\delta = +1.9$ ppm) are indicated.

Double-Quantum ^{1}H MAS NMR Sideband Analysis. If the 2D DQ MAS experiment is performed with shorter nonrotor-synchronized t_1 increments, a 2D spectrum is obtained where a spinning sideband pattern is observed in the DQ dimension. Figure 3 shows the 1D slices of the nonrotor-synchronized DQ MAS spectra for compound (**I**) for the two different ^{1}H chemical shifts. The 1D ^{1}H DQ sideband pattern obtained for the ^{1}H resonance at $\delta = +1.9$ ppm is shown in Figure 3a, while the DQ sideband projection for the H_2O resonance ($\delta = +6.3$ ppm) is shown in Figure 3b. These DQ sideband patterns are very sensitive to the effective dipolar coupling strength D^{ij}_{eff} between the protons in the system and the excitation−recoupling durations. The DQ sideband simulations assuming an isolated two-spin pair are shown as dashed lines in Figure 3.

Solid-State ^{1}H−^{93}Nb MAS TRAPDOR NMR. Figure 4a shows the effect of ^{93}Nb irradiation on the rotor-synchronized ^{1}H MAS spin−echo experiment of compound (**I**) at 20 kHz. These ^{1}H−^{93}Nb TRAPDOR experiments allow for the detection of weak heteronuclear dipolar coupling between spins. Figure 4b shows the variation of the TRAPDOR fraction $[(S_0 - S)/S_0]$ as a function of mixing time for both the $\delta = +6.3$ ppm and $\delta = +1.9$ ppm resonance in (**I**). At short irradiation times, the TRAPDOR fraction of the $\delta = +1.9$ ppm resonance reveals a larger increase due to the ^{93}Nb irradiation than the $\delta = +6.8$ ppm resonance, but at longer irradiation times the TRAPDOR fractions for the two ^{1}H resonance become equivalent.

Solid-State ^{17}O MAS NMR. The solid-state ^{17}O MAS NMR spectra obtained for the ^{17}O-labeled version of (**I**) at 81.40 MHz for spinning speeds of 35 kHz is shown in Figure 5a, with an

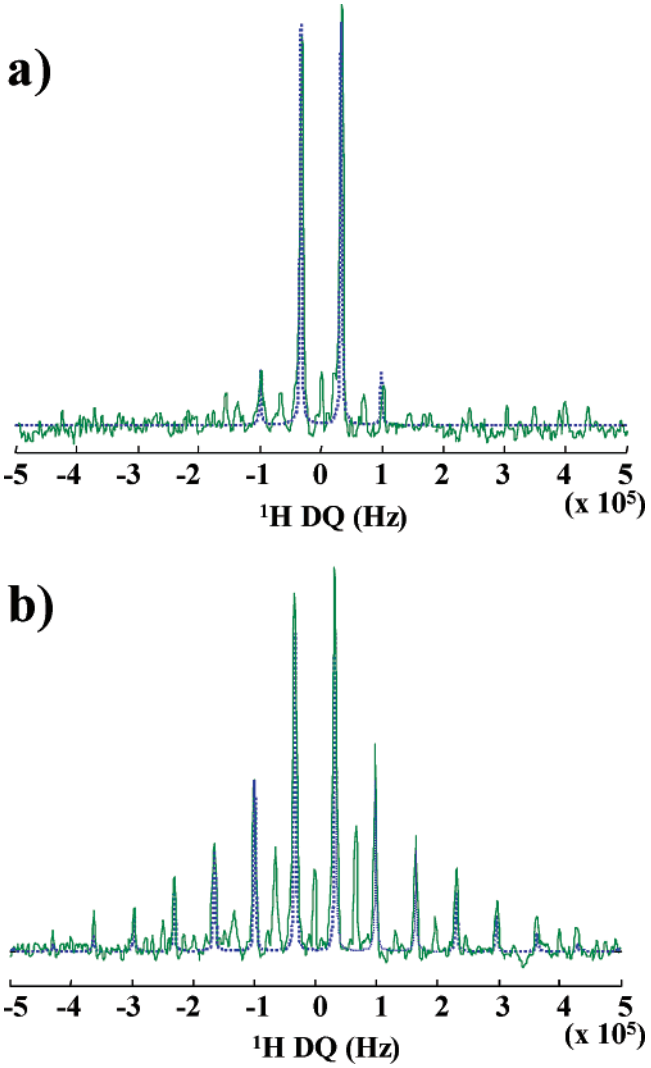

Figure 3. 1D DQ ^{1}H spinning sideband projections for the proton resonance at (a) $\delta = +1.9$ ppm and (b) +6.3 ppm. The DQ sideband simulations (− − −) were obtained using a two-spin approximation (eq 1) using a distribution of effective dipolar couplings. See additional discussion in text.

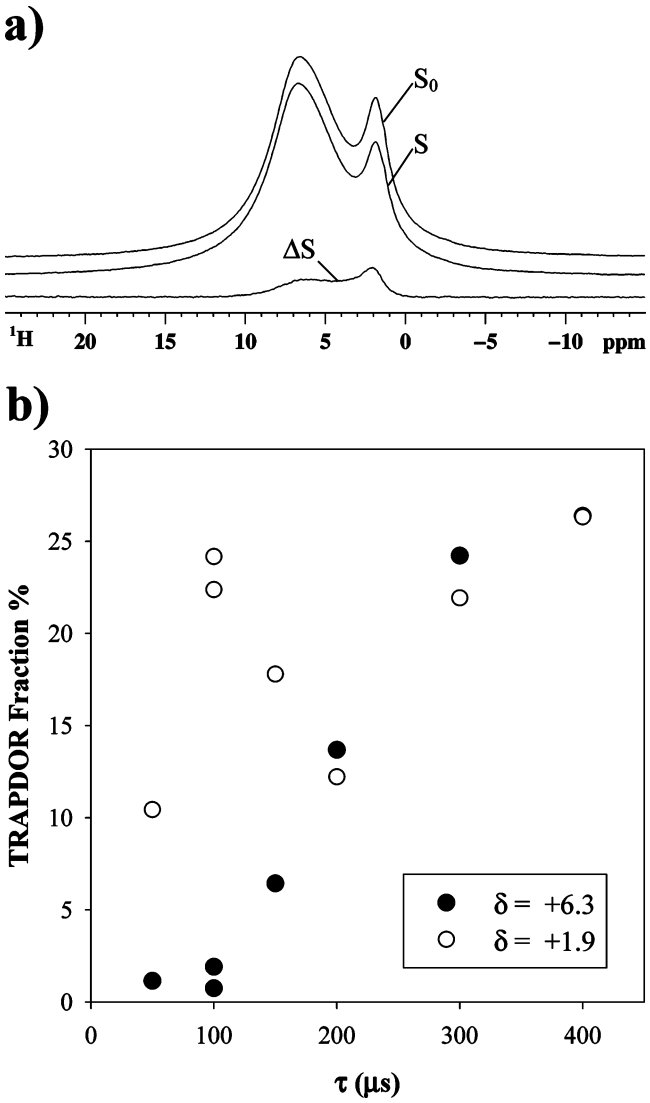

Figure 4. (a) ^{1}H−^{93}Nb TRAPDOR spectra for (**I**) using the rotor-synchronized irradiation time of $\tau = N\tau_r$, where N is the number of rotor periods ($N = 4$) and τ_r is the rotor period ($\tau_r = 100$ μs). The spectra from the spin−echo experiment without ^{93}Nb irradiation (S_0), with ^{93}Nb irradiation (S), and the difference spectra (ΔS). (b) The variation of the TRAPDOR fraction ($\Delta S/S_0$) for the two ^{1}H resonances at $\delta = +6.8$ and +1.9 ppm as a function of τ.

expansion of the isotropic peak region in Figure 5b. The ^{17}O MAS NMR spectra at 54.28 MHz using a 15 kHz spinning speed is shown in Figure 5S (Supporting Information). The different isotropic resonances and associated spinning sidebands are designated. The observed ^{17}O chemical shifts and assignments are given in Table 1. The Nb_2O−H and Nb_6O_C (protonated bridging oxygen and central oxygen, respectively) resonances are partially obscured in Figure 5b by spinning sidebands of other resonance, but can be distinguished in spectra at different spinning speeds or field strengths (see Figure 5S). No significant change in the resonance positions with changes in the field strength were observed, showing that large second-order quadrupolar induced isotropic shifts are not present in (**I**). The ^{1}H−^{17}O CPMAS NMR spectrum (54.28 MHz) is shown in Figure 5c. The CPMAS spectrum shows a very broad resonance for the H_2O species and probably corresponds to those immobile, tightly bound water species that retain significant CP efficiency. The CP buildup of the bridging oxygen resonance ($\delta = +386$ ppm) as a function of CP contact time is very rapid (Figure 6S in Supporting Information), showing a maximum at ~150 μs, but rapidly building up to ~93% of maximum intensity in 60 μs. Similar oscillations at these short contact times have previously been observed in the ^{1}H−^{17}O CPMAS buildup of polycrystalline $Ca(OH)_2$.[39] Solid-state 2D ^{1}H−^{17}O CPMAS NMR correlation spectra for compound (**I**) are shown in Figure 6.

Solution ^{17}O NMR. The solution ^{17}O NMR spectra as a function of time for the ^{17}O-labeled (**I**) dissolved in natural abundance water are shown in Figure 7a,b. Five distinct resonances corresponding to the four different oxygen types in (**I**) and a ^{17}O resonance for the associated H_2O were observed. The chemical shifts and line widths for these different ^{17}O resonances as a function of temperature and pH are given in Table 1. The ^{17}O NMR assignments were based on previous literature.[17,22,23,28−31] It is clear from Figure 7 that exchange between the different ^{17}O-labeled oxygen environments within the compound and the unlabeled oxygen of the H_2O solvent is occurring. The loss of signal intensity for the different oxygen species as a function of time at different temperatures and pH

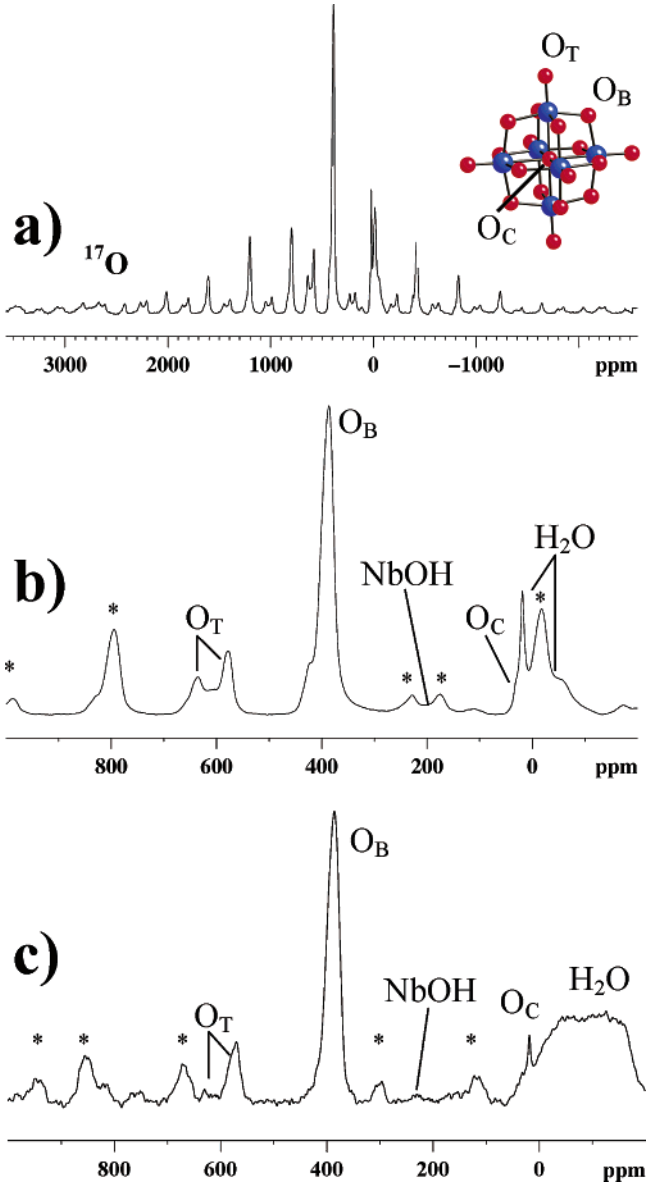

Figure 5. Solid-state ^{17}O MAS spectrum for (**I**) at (a) 81.40 MHz, spinning speed of 35 kHz, (b) an expanded spectrum of the central isotropic peak region, and (c) isotropic region for ^{17}O CPMAS NMR spectrum obtained at 54.28 MHz, spinning speed of 15 kHz. The isotropic resonances are marked, while the associated spinning sidebands are denoted by *. The different oxygen species corresponding to the $[Nb_6O_{19}]^{8-}$ Lindquist ion (inset) are denoted.

is shown in Figure 8a−d. In general, it is difficult to correctly quantify the relative peak areas for resonances with widely different line widths and oxygen exchange rates, such that the relative ratios are not reported. The incorporation of ^{17}O into unlabeled (**I**) can also be accomplished by dissolving the compound in ^{17}O-enriched H_2O and following as a function of time. An example spectrum for this process is given in the Supporting Information (Figure 7S).

Discussion

Characterization of ^{1}H Environments. The ^{1}H MAS NMR spectra in Figure 1 reveal two distinct proton environments in compound (**I**). The observation of two distinct ^{1}H resonances in the ^{1}H MAS NMR also demonstrates that rapid exchange of protons between these different environments is *not* occurring on the NMR time scale given by the peak separation (∼3000 Hz), even though slower exchange processes may be occurring (see below). There have been numerous ^{1}H MAS NMR studies investigating the proton environments in zeolite systems.[14,42] There have been few solid-state ^{1}H NMR studies of polyoxoniobate materials reported.[43] In zeolites, the ^{1}H chemical shift of the hydroxyl proton has been reported between +1.3 and +2.2 ppm for SiOH,[42,44] −0.2 ppm for AlOH hydroxyls,[42] and +1.3 ppm for TiOH.[45] The ^{1}H chemical shifts of bridging hydroxyl in zeolites (SiOHAl) are a function of framework Si/Al ratios, and range between +3.8 and +4.3 ppm. In niobium oxide hydroxyl protons have been observed between $\delta = +1.5$ and +2.9 ppm.[43] Physisorbed water chemical shifts in zeolites are typically reported between +3.5 and +4.9 ppm,[44] while H_2O molecules adsorbed to Bronsted acid sites have been reported between +6.0 and +6.9 ppm.[14,42] In niobium oxide, the water protons in rapid exchange with acid and hydroxyl protons have been reported between $\delta = +5.1$ and +6.4 ppm.[43] It is generally argued that the DQF and T_2-filtered ^{1}H MAS NMR experiments preferentially suppress the signal from mobile or strongly dipolar-coupled protons, respectively. On the basis of the differential response during the filtering experiments, the resonance at $\delta = +6.3$ ppm is assigned water adsorbed to either a Lewis or Brønsted acid site within compound (**I**). The ^{1}H NMR chemical shift for this H_2O resonance was larger than that observed for physisorbed H_2O in zeolites. The observed ^{1}H NMR chemical shift is similar to the chemical shift of H_2O associated with the Brønsted acid site in zeolites and may reflect the highly charged nature of the niobate cluster.[43,46] The mobility of a large fraction of the H_2O molecules ($\delta = +6.3$ ppm) in compound (**I**) is highly restricted (see DQ sideband discussion below) and are consistent with strong interactions between the niobium-oxo cluster and the H_2O species. The narrow ^{1}H NMR resonance at $\delta = +1.9$ ppm is tentatively assigned to a niobium hydroxyl (Nb−O−H) proton species. This assignment is further supported by the solid-state IR spectra of $Na_7[HNb_6O_{19}]\cdot 15H_2O$ (Figure 8S, Supporting Information). Below 1000 cm^{-1} the vibrational modes of the niobium-oxo cluster are observed, along with the Na−O vibrational modes of the water-bound and cluster-bound sodium atoms. The broad bands around 3300 and 1800 cm^{-1} are, respectively, the stretching and bending modes of water. The small but sharp peak at ∼3500 cm^{-1} is characteristic of the stretching mode of a hydroxyl bound to a metal such as niobium (NbO−H).[47]

Characterization of Dipolar Interactions. Additional information about the ^{1}H environment can be obtained from the 2D ^{1}H DQ NMR exchange results (Figure 2) and the ^{1}H−^{93}Nb TRAPDOR experiment (Figure 4). The lack of an autocorrelation peak in the 2D DQ NMR exchange experiment for the $\delta = +1.9$ ppm demonstrates that this proton species is isolated from protons in similar environments. This is consistent with a NbOH species, since the molecular structure ($Na_7[HNb_6O_{19}]\cdot 15H_2O$) predicts only a single proton per hexaniobate cluster,

(42) Hunger, M. *Solid State Nucl. Magn. Reson.* **1996**, *6*, 1−29.
(43) Batamack, P.; Vincent, R.; Fraissard, J. *Catal. Lett.* **1996**, *36*, 81−86.
(44) Kinney, D. R.; Chaung, I.-S.; Maciel, G. E. *J. Am. Chem. Soc.* **1993**, *115*, 6786−6794.
(45) Leboda, R.; Turov, V. V.; Marciniak, M.; Malygin, A. A.; Malkov, A. A. *Langmuir* **1999**, *15*, 8441−8446.
(46) Iizuka, T.; Ogaswara, K.; Tanabe, K. *Bull. Chem. Soc. Jpn.* **1983**, *56*, 2927−2931.
(47) Nakamoto, K. *Infrared and Raman Spectra of Inorganic and Coordination Compounds*, 5th ed.; John Wiley & Sons: New York, 1997.

Table 1. Solution and Solid-State ^{17}O NMR Spectral Data for $Na_7[HNb_6O_{19}]\cdot 15H_2O$[a]

sample	chemical shifts, ppm[b] (line widths, Hz)				
	O_T	O_B	NbOH	O_C	H_2O
		Solution (°C)			
20[c]	631 (260)	376 (1720)	186 (250)	34 (100)	0 (170)
30[c]	633 (230)	375 (1330)	185 (230)	35 (100)	0 (170)
50[c]	633 (225)	375 (620)	186 (180)	36 (120)	−1 (150)
20[d]	633 (225)	372 (1350)	182 (225)	34 (100)	0 (170)
20[e]	630 (225)	376 (1000)	186 (250)	33 (120)	0 (180)
30[e]	633 (250)	375 (800)	186 (250)	35 (100)	0 (150)
50[e]	632 (300)	375 (650)	187 (215)	36 (150)	−1 (180)
		Solids (°C)			
25 (54.28 MHz)	631 (1100)[f,g] 575 (1175)[f,g]	386 (1450)[f] [426][f,g]	226 (700)	31 (330)[f]	18 (275)[f] [−90 (9000)][h]
25 (81.40 MHz)	636 (1600)[f,g] 576 (1700)[f,g]	386 (2100)[f] [423][f,i]	227 (1500)	31 (500)[f]	19 (800)[f]

[a] See Experimental Section for additional spectral parameters. [b] ^{17}O chemical shifts reported with respect to secondary external reference of pure H_2O at 298 K ($\delta = 0.0$ ppm). Line widths refer to full width at half-maximum (fwhm) in Hz. [c] Sample dissolved in a phosphate buffer, pH = 7.4. [d] Sample dissolved in a Na_2CO_3 buffer, pH = 10.0. [e] Sample dissolved in distilled H_2O, where the final pH = 11.0, as measured by a pH meter. [f] Observed ^{17}O chemical shift. No correction for second-order quadrupolar coupling isotropic shift made. [g] Two nonequivalent oxygen environments were observed for this site. [h] An extremely broad H_2O resonance (>9000 Hz) was observed under CP conditions. [i] A weak shoulder was observed for this resonance in the solid state.

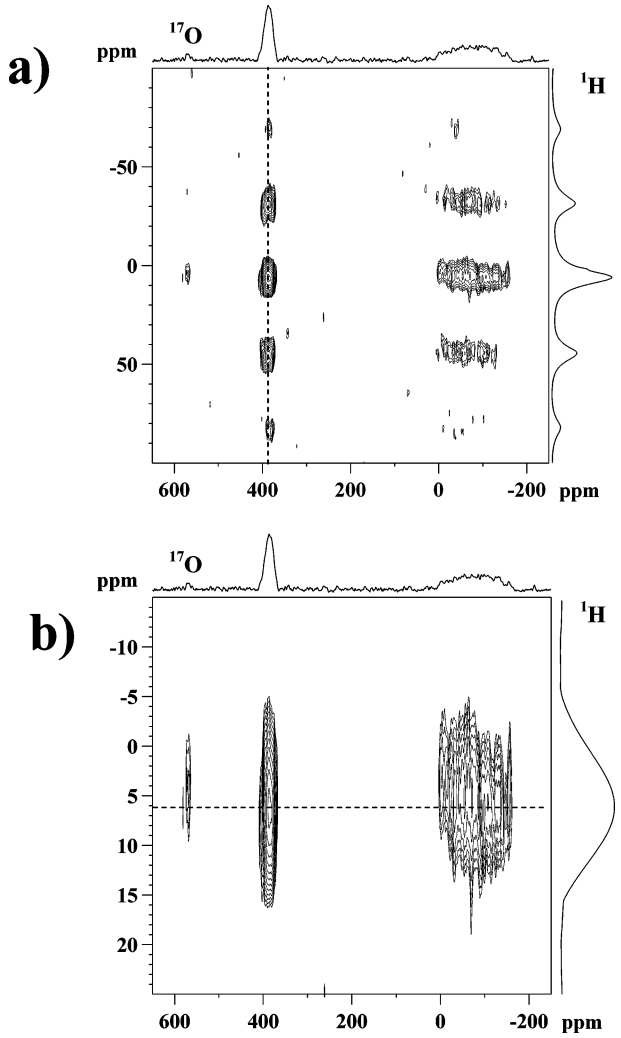

Figure 6. (a) Full 2D $^1H-^{17}O$ MAS NMR correlation spectrum for (**I**). (b) The expansion of the isotropic resonance, where the dashed horizontal line shows the strong correlation with the ^1H resonance at $\delta = +6.3$ ppm (H_2O).

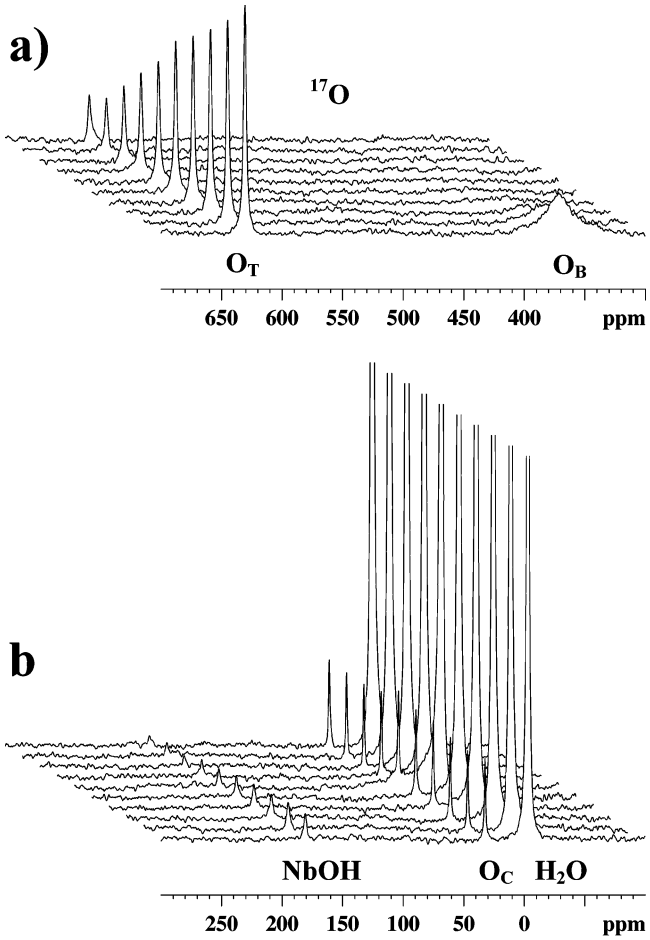

Figure 7. Solution ^{17}O NMR spectra for ^{17}O-labeled (**I**) dissolved in unlabeled phosphate buffered (ph = 7.4) solution as a function of time at 30 °C.

and the clusters are separated by sodium and water species. The lack of an autocorrelation resonance in the DQ NMR spectra also shows that long-range dipolar interactions between protons of different $[HNb_6O_{19}]^{-7}$ clusters via NbOH species are not occurring in the solid state. The DQ cross-peak between the $\delta = +6.3$ and the $\delta = +1.9$ ppm proton species shows they are spatially related and are in a single phase, in contrast to the multiple phases observed in the NMR investigations of the Keggin heteropoly acids $H_3PMo_{12}O_{40}$ and $H_3PW_{12}O_{40}$.[32]

The DQ ^1H MAS NMR spinning sidebands are sensitive to changes in the strength of the $^1H-^1H$ dipolar interaction. Using eq 1, we determined an effective dipolar coupling for the $\delta =$

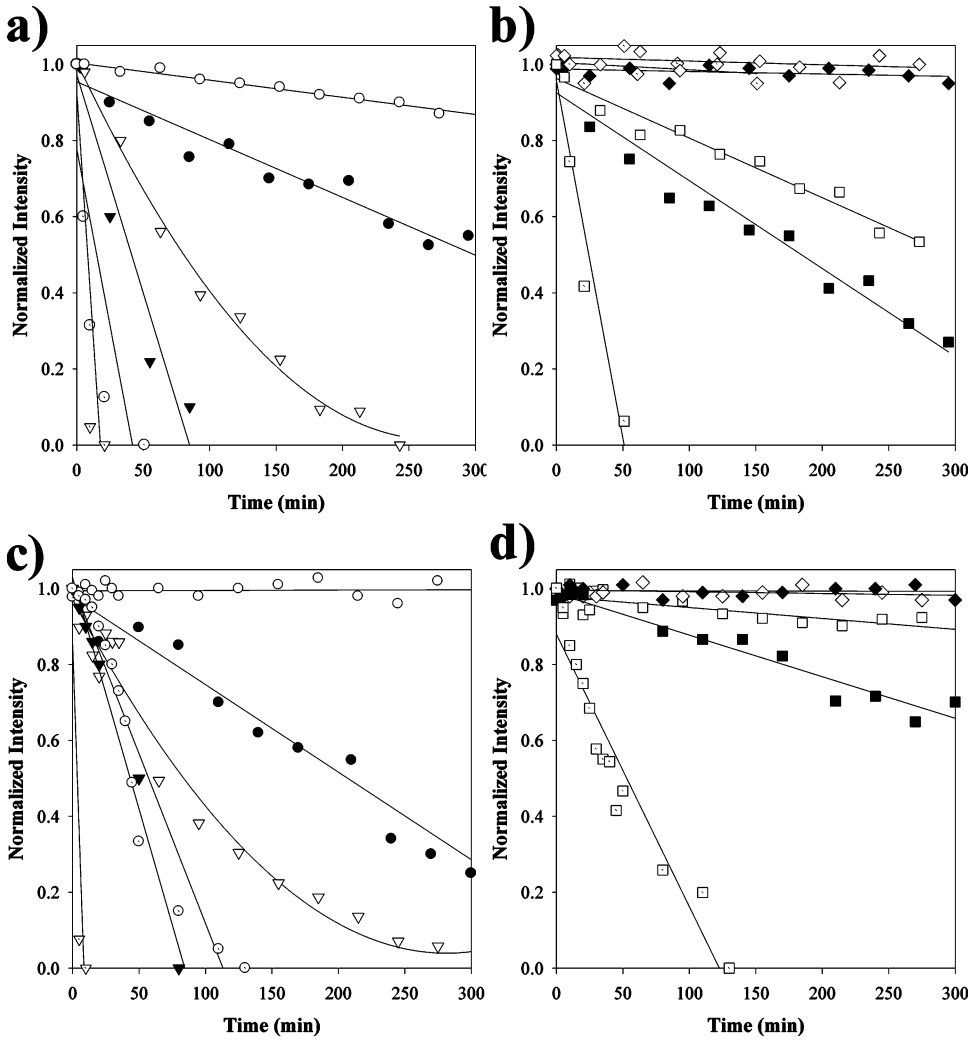

Figure 8. Variation of the ^{17}O NMR signal intensity of compound (**I**) in solution with exchange time and temperature. The intensity variation of (a) the bridging (O_B) and hydroxyl (NbOH) oxygen, (b) the terminal (O_T) and central (O_C) oxygen environments at pH = 7.4, (c) the O_B and NbOH oxygen, and (d) the O_T and O_C oxygen environments at pH = 11.0. In all plots, the intensities of the O_B NMR signal are denoted by (▽,▼,⊽), NbOH by (○,●,⊙), O_T by (□,■,⊡), and O_C by (◇,◆,⟐) for 20, 30, and 50 °C, respectively.

+6.3 ppm resonance (H_2O) to be 23 ± 1 kHz, with a dipolar coupling distribution of σ ± 4.8 kHz.[48] The δ = +1.9 ppm resonance (NbOH) has an effective dipolar coupling of 5.5 ± 1 kHz, with no significant distribution ($\sigma \approx 0$ kHz). It is interesting to note that the DQ sideband spectra for the water resonance requires a large distribution of D^{ij}_{eff} consistent with the multiple waters in the crystal lattice, as well as the dynamic nature of these water species.

In a rigid water molecule, the dipolar coupling is calculated to be 33.4 kHz,[49] using eq 2 and assuming an interproton distance of 1.54 Å. Molecular motions of the water will produce an averaged effective dipolar coupling (D^{ij}_{eff}), allowing a measure of the motional order parameter (S) using

$$S = \frac{D^{ij}_{\text{eff}}}{D^{ij}} \qquad (3)$$

From the observed D^{ij}_{eff} of the H_2O resonance (δ = +6.3 ppm), the calculated order parameter of S = 0.69 clearly shows that the water molecules in compound (**I**) observed in the DQ experiments have very low mobility.

The ^1H resonance at δ = +1.9 ppm (NbOH) also reveals DQ spinning sidebands, but the magnitude of the dipolar coupling is much smaller, showing that the hydroxyl protons are only weakly coupled to other protons within the crystal lattice. It might be argued that the small dipolar interaction for the δ = +1.9 ppm resonance is due to very rapid motional averaging in this species. The DQF ^1H MAS NMR experiments (Figure 1b−d) argue against this, since the δ = +1.9 ppm resonance shows the least amount of signal suppression during the excitation−conversion portion of the BABA sequence. This trend in signal intensity is opposite the large decrease in the DQ intensity predicted due to rapid motional averaging of the dipolar coupling. It has also been suggested that a portion of the signal suppression for the δ = +6.3 ppm resonance may result from interference effects of molecular motions of these

(48) The distribution width, σ, reported here differs from that previously reported in ref 41. In the present study, we have elected to use a more standard formulation describing the distribution of effective dipolar couplings, $\rho_I(D) = 1/\sqrt{2\pi}\exp[-(\bar{D}^{ij} - D_I^{ij})^2/2\sigma^2]$. The full width at half-maximum of the distribution is now defined by $2\sqrt{2\ln 2}\sigma \approx 2.35\ \sigma$. The widths obtained using these two different definitions of the dipolar distribution are related by a simple scaling factor of $\sqrt{2}$.

(49) Abragam, A. *Principles of Nuclear Magnetism*; Oxford University Press: New York, 1961.

H_2O species on the time scale of the BABA pulse sequence, making this simple argument based on differential intensity loss less substantial. Nevertheless, we feel that the small D^{ij}_{eff} observed for the $\delta = +1.9$ ppm demonstrates that this proton species is isolated from similar species and is only weakly coupled to the nearby H_2O protons in the crystal lattice.

For an isolated spin pair it is known that the DQ sidebands described by eq 1 should be symmetric and only occur at odd multiples of the MAS frequency. Multispin dipolar interactions, or large chemical shift anisotropy (CSA), can lead to the generation of even-ordered spinning sidebands through an evolution rotor modulation (ERM) mechanism.[34] While the intramolecular dipolar interaction for H_2O is expected to be dominant, close analysis of the DQ sidebands reveals that multispin intermolecular interactions are also occurring since even-ordered sidebands are observed. For compound (**I**), the DQ sideband NMR spectra (Figure 3) is asymmetric. The asymmetry is more notable for the DQ spectra obtained for BABA sequences with excitation−reconversion periods of τ_R and $2\tau_R$ duration. These excitation−reconversion sequences are not fully compensated for chemical shift offset effects, while the $4\tau_R$ sequence is compensated to zero order.[33] It has been previously observed that large ^{1}H CSA can give rise to asymmetric DQ sideband patterns,[50−52] but the ratio of the average sideband intensities are virtually unchanged.[51] Considering the error introduced by the multispin interactions and the presence of a significant ^{1}H CSA effect, it is estimated that the uncertainty in the determination of the effective dipolar coupling for the two proton species is on the order of ±1 kHz.

The ^{1}H−^{93}Nb TRAPDOR fraction buildup (Figure 4) at short irradiation times shows that the ^{1}H resonance at $\delta = +1.9$ ppm possesses a stronger dipolar coupling to niobium than the H_2O species at $\delta = +6.8$ ppm, which is consistent with the assignment of the $\delta = +1.9$ ppm resonance as a Nb−OH species. At longer echo times, the TRAPDOR fraction for the two different ^{1}H species becomes equivalent, suggesting that there is proton exchange between the hydroxyl proton and protons in H_2O occurring on the order of ∼200 μs. This TRAPDOR result, along with the weak ^{1}H−^{1}H dipolar coupling associated with the $\delta = +1.9$ ppm ^{1}H species, provides an additional argument *against* this resonance being an isolated H_3O^+ cluster species (see structure A). This type of coordinated H^+ structure was previously proposed for the heteropoly acid hydrate $H_3PW_{12}O_{40}\cdot 6H_2O$.[24,25] For structure 1A, a strong dipolar interaction between the H+ and the protons of the neighboring H_2O would be predicted and, therefore, would be observed in the DQ sideband analysis. In addition, the heteronuclear dipolar interaction between the proton and niobium nuclei would be predicted to be larger for the associated H_2O species than that of the spatially removed H^+ species. This was not observed experimentally. It has also been argued that a fraction of the total observed H_2O species (15 total H_2O per cluster) are indeed coordinated as structure A. The TRAPDOR response of this small fraction of coordinated H_2O species would be difficult to distinguish from the other uncoordinated H_2O species (which may be more mobile and spatially removed from the Nb nuclei). This would produce a superposition of the different TRAPDOR responses for the different ^{1}H fractions. Under this assumption, the longer echo times in the TRAPDOR should preferentially select signal from the closely coordinated H_2O species described by structure A due to their reduced mobility. The close proximity to niobium for this select fraction would result in an increase in the TRAPDOR signal at the longer echo times to values larger in magnitude than that observed for the $\delta = +1.9$ ppm resonance. Conversely, if there was a preferential selection of the noncoordinated H_2O (more mobile) fraction, the TRAPDOR curve for the $\delta = +6.3$ ppm resonance would show a decrease at longer echo times. Neither of these variations in the TRAPDOR buildups is observed (Figure 4). The only abrupt variation was the decrease in the TRAPDOR fraction for the $\delta = +1.9$ ppm resonance at longer mixing times. The TRAPDOR results are consistent with the H_3O^+ (structure B) observed by Goiffon et al. in the crystal structure of $H_3O\cdot Na_7[Nb_6O_{19}]\cdot 14H_2O$. The hydrogen is associated primarily with the water (i.e., the H_3O designation) and has a weak bonding interaction to the bridging oxygen in the niobate cluster. In the crystal structure, a water molecule is located 2.7 Å from a bridging oxygen of the cluster, which is close enough to provide a weak bonding interaction. Structure B would predict an increased dipolar interaction between the proton and niobium compared to the water−niobium dipolar interaction, as was observed in the TRAPDOR NMR experiments. These observations support the assignment of the $\delta = +1.9$ ppm ^{1}H NMR resonance as a Nb−OH proton species either at the terminal oxygen position or at the bridging oxygen. NMR experiments to help define the location of the NbOH species are below.

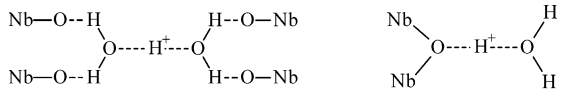

A **B**

Characterization of the ^{17}O Environments. In both the solid-state and solution ^{17}O NMR, resonances corresponding to the terminal (O_T), bridging (O_B), hydroxyl (NbOH), and central oxygen (O_C) for the niobium Lindquist cluster, $[Nb_6O_{19}]^{8-}$, are observed (see Table 1). These assignments are based on previous ^{17}O NMR studies of polyoxometalates.[22−27] For the $[Nb_6O_{19}]^{8-}$ hexaniobate anion in solution, ^{17}O NMR chemical shifts of +594, +386, and +20 ppm have been reported for the ONb, ONb_2, and the ONb_6 oxygens by English and coworkers.[15] In a later study, by Filowitz et al.,[18] ^{17}O NMR chemical shifts of +607, +392, and +29 ppm were observed for the $[Nb_6O_{19}]^{8-}$ anion in solution. A ^{17}O NMR chemical shift of +493 ppm for the ONb oxygen environment has also been reported for the $[Nb_2W_4O_{19}]^{4-}$ anion in water. The solution ^{17}O NMR shift of hydroxyl species (NbOH) in niobium-oxo materials has been reported between $\delta = +180$ and 187 ppm.[28,30,31] As noted previously, accurate quantification of the different ^{17}O resonances is difficult due to the significantly different line widths and oxygen-exchange rates. Nevertheless the NbOH/O_C peak ratios (immediately after mixing) were found to range from 1.0 to 1.3 for the pH ranges investigated, consistent with the assignment of the NbOH resonance.

In the solid-state ^{17}O NMR, the O_T species are nonequivalent (Figure 5) and show two resonances at $\delta = +636$ and +576

(50) Tekely, P.; Demco, D. E.; Canet, D.; Malveau, C. *Chem. Phys. Lett.* **1999**, *309*, 101−110.
(51) Brown, S. P.; Zhu, X. X.; Saalwächter, K.; Spiess, H. W. *J. Am. Chem. Soc.* **2001**, *123*, 4275−4285.
(52) De Paul, S. M.; Saalwachter, K.; Graf, R.; Spiess, H. W. *J. Magn. Reson.* **2000**, *146*, 140−156.

ppm in an approximate 1:2.5 ratio. This corresponds with the two O_T in a 2:1 ratio located in the solid-state structure of $Na_7[H_3O^+Nb_6O_{19}]\cdot 14H_2O$ as determined from single-crystal X-ray data.[3] One O_T is within bonding range of one Na, and the second is within bonding range of two Na (Na−O bond < 2.7 Å). The O_T ^{17}O chemical shift is ∼25 to 38 ppm larger than solution ^{17}O shifts previously reported in the literature. The O_B oxygen has a single resolvable resonance at $\delta = +386$, which is +10 to +12 ppm larger than observed in solution. This increase in the ^{17}O chemical shift can be related to an increase in the Nb−O bond strength.[22] In the solid state, the ^{17}O chemical shift for the NbOH species is observed at +226 ppm and is ∼+40 ppm larger than that observed in solution (Table 1). The downfield shift of the NbOH resonance suggests that the Nb−O bond strength is larger and that the extent of the proton interaction is reduced in solid state versus solution.[22] Both a sharp resonance and a very weak broad ^{17}O NMR resonance are observed for the adsorbed water in the direct ^{17}O MAS NMR spectra, while in the $^1H-^{17}O$ CPMAS NMR spectrum only a very broad resonance (∼9000 Hz) for the H_2O is observed (Figure 5c). These differences suggest that there are both H_2O species that are rather mobile (and possess a very poor CP efficiency) and H_2O species that are rigid or tightly bound (with good CP efficiency). This is again consistent with the structure from X-ray diffraction: one water molecule in the unit cell is located within H-bonding range of the cluster oxygens, and three water molecules are out of bonding range with the cluster, with an $O_{cluster}-O_{water}$ distance >4 Å. The relative ratio of the water resonances in Figure 5 is reduced since the crystals of the ^{17}O-labeled (**I**) were quickly washed with unlabeled water to reduce the dominating ^{17}O signal from the coordinated water species. This rinsing with unlabeled water may have resulted in differential back exchange of the ^{17}O label incorporated into (**I**) with unlabeled oxygen, as observed in the solution exchange experiments (see below). Long-term storage of these ^{17}O-labeled samples of (**I**) did not result in a significant increase of the ^{17}O-labeled water resonance observed in the direct ^{17}O MAS NMR spectra, demonstrating that oxygen exchange is relatively slow in the solid state under storage conditions.

In the solution ^{17}O NMR experiments there are large differences in the line widths observed (Table 1), with $O_B \gg O_T \approx$ NbOH > O_C. In previous studies of polyoxometalates, the differences in the ^{17}O line widths were related to spin−spin and spin−lattice relaxation changes.[18,19] It had been argued that the symmetric O_C would have the smallest quadrupolar coupling constant (QCC) and, therefore, the smallest relaxation rates, producing the narrowest lines. Differential oxygen exchange rates (see below) may also contribute to the differences in line width noted, precluding arguments about the magnitude of QCC from observed line width trends.

Location of the Protons. On the basis of ^{17}O NMR chemical shift arguments, it is demonstrated that the NbOH is located on a bridging oxygen in both the solid state and solution for compound (**I**) (structure B). In solution, the NbOH resonance did not show any large variations with pH. Previous ^{17}O NMR studies in oxovanadium materials have used the variation of chemical shift with pH as a measure of the protonation site.[22] For compound (**I**), the small variation in the NbOH ^{17}O chemical shift with pH (Table 1) shows that this OH bond is not significantly weakened between pH 7.2 and 11.0. In the solid state a very weak intensity buildup for the NbOH species unfortunately is observed in the $^1H-^{17}O$ CPMAS experiments, most likely resulting from rapid ^1H exchange with the water species. This exchange was also responsible for the averaging observed in the $^1H-^{93}Nb$ TRAPDOR buildups. This lack of significant CP efficiency precludes the use of the $^1H-^{17}O$ CPMAS results from supporting the chemical shift assignments. No correlations with the hydroxyl resonance at $\delta = +1.6$ ppm is observed in the 2D $^1H-^{17}O$ correlation experiments, also due to this poor CP efficiency.

Interestingly, the $^1H-^{17}O$ CPMAS spectrum in Figure 5c shows that the O_B oxygen species were closely coupled to protons. The rapid CP build up of O_B resonance (Figure 4S, Supporting Information) is also consistent with closely coupled protons. The 2D $^1H-^{17}O$ MAS NMR correlation spectrum in Figure 7 shows that these O_B are strongly correlated with the ^1H resonance of H_2O at $\delta \approx +6.3$ ppm. It was shown in the DQ experiments (see above) that the H_2O species have very low dynamic mobility, consistent with a strong binding interaction. The strong $^1H-^1H$ dipolar coupling in these protons is also evident by the strong spinning sideband pattern observed in Figure 6a (vertical dashed line), consistent with the assignment of an immobile H_2O species. The correlation experiments show that the O_T resonance at $\delta = +631$ ppm exhibits no dipolar interactions with ^1H, while the O_T resonance at $\delta = +576$ ppm reveals a weak dipolar interaction with the ^1H resonance at $\delta \approx +3.6$ ppm. This new ^1H resonance is not resolved in the direct ^1H MAS NMR, even though there is some asymmetry observed for the $\delta = +6.3$ ppm resonance in the T_2-filtered MAS NMR spectra (Figure 2f−h). The lack of a strong ^1H spinning sideband pattern for this resonance in Figure 6a shows that there exists very little $^1H-^1H$ dipolar coupling for this new proton species. This resonance probably arises from a water species in the crystal lattice with intermediate mobility. This is also consistent with powder XRD characterization of different synthesized samples of compound (**I**), where slight changes in structure as a function of synthesis conditions (hydrothermal vs open beaker) have been noted. We have attributed these structural variations to differences in the crystal lattice hydration. These 2D NMR results show that the H_2O within the crystal lattice is *not* strongly associated with the O_T oxygens, but are preferentially strongly associated with the O_B species.

4.4. Oxygen Exchange and Rearrangement in Hexaniobate Clusters in Solution. The rate of oxygen exchange in compound (**I**) in solution was investigated by dissolving the ^{17}O-labeled compound in unlabeled water and following the changes in the solution ^{17}O NMR signal intensity as a function of time (Figure 8a−d). These kinetic experiments were determined for three different temperatures (20, 30, and 50 °C) at pH = 7.4 (Figure 8a,b) and pH = 11.0 (Figure 8c,d). The pH = 7.4 solution was achieved using a phosphate buffer, and the pH = 11.0 solution was obtained by simply dissolving compound (**I**) in DI water. Both solutions were 5 mM concentration of compound (**I**). At room temperature, the relative rate of exchange is $O_B \gg O_T >$ NbOH $\gg O_C$. For the pH and temperature values investigated, the central O_C oxygen reveals almost no exchange with the unlabeled solvent during the course of the experiment. Extended experiments at 50 °C reveal no appreciable signal loss from the O_C oxygen through ∼24 h. Analogous differential oxygen

exchange effects have been noted in previous polyoxometalate studies.[18] The O_T, O_B, and NbOH oxygen all show appreciable variation in exchange rate with temperature. The exchange rate of the O_B species varies little with pH, while both the NbOH and O_T exchange rates are reduced at higher pH at room temperature (Figure 8c,d). The reduction of the exchange rate for the NbOH species with increasing pH is reversed for temperatures >30 °C. The temperature variation of the NbOH is greater than the O_T oxygen at pH = 7.4, but this differential temperature dependence is reduced at pH = 11.0 (Figure 8). From these kinetic experiments, it appears that the mechanism of exchange for the multiple oxygen environments is different. The differential exchange rates, plus differential response to pH and temperature variations for oxygen exchange/rearrangement in the hexaniobate Lindquist anions, are discussed below.

The central Nb_6O_C oxygen shows very slow oxygen exchange under the conditions investigated, suggesting that the cluster geometry is preserved and that all other oxygen exchange mechanisms take place without disrupting the Nb−O_C bond. The ^{17}O NMR spectra of the Lindquist ion in aqueous solution clearly show that the O_B site is the favored site for proton attachment. The bridging oxygen site also undergoes the fastest oxygen exchange with water, yet the exchange rate of this O_B position, while affected significantly by temperature, is not affected by pH. This suggests that protonation of the O_B site is not a rate-determining step in the exchange process, or perhaps is not even involved in the exchange mechanism. The observation of the NbOH exchange rate being slower than the O_B exchange rate also demonstrates that NbOH is not directly involved in the O_B exchange process. The oxygen exchange rate of the O_T terminal site is comparable with that of the Nb−OH site, with the exchange rate increasing at lower pH. Both the O_T and NbOH sites show similar variation with pH, with the NbOH oxygen exchange rate showing a much higher variation with temperature. These results (Figure 8) suggest that in contrast to the O_B site, protonation of the oxygen is involved in the oxygen-exchange mechanism for the NbOH and O_T sites. The dimerization of the hexaniobate, a process that is favored in acidic solutions, is one possible mechanism for the oxygen exchange for O_T and NbOH site.[1] Dimerization does not explain the O_B site having significantly faster exchange rates. At pH < 7, $[Nb_6O_{19}]^{8-}$ in solution begins to decompose and precipitate an amorphous, hydrous niobium oxide. Formation of larger clusters such as the dodecaniobate may very well be an intermediate step to this process. The differential exchange rates are also consistent with the observed differences in line width, with the magnitude of the line widths being $O_B \gg O_T \approx$ NbOH > O_C (see Table 1). The line width of the O_B resonance shows the largest response to variations in temperature, consistent with a rapid exchange process occurring at this position. It appears that the observed line width may involve exchange broadening and not simply difference in the spin relaxation rate due to changes in the magnitude of QCC for the different oxygen sites.

5. Summary

We have demonstrated that the environment, location, and dynamics of the protons and oxygens in the monoprotic hexaniobate material, $Na_7[HNb_6O_{19}]\cdot 15H_2O$, can be determined using multinuclear NMR techniques. These investigations show that the location of the proton is the bridging oxygen (O_B) of the $[Nb_6O_{19}]^{8-}$ Lindquist ion in both the solid state and solution and confirms previous postulations that this is the most basic oxygen site. The 2D DQ ^1H NMR dipolar exchange experiments show that this proton is isolated from similar proton species. These solid-state NMR experiments also reveal that the H_2O species in this structure have restricted dynamics and are associated preferentially with the O_B oxygens in the hexaniobate. In solution there is rapid exchange of the oxygens with the solvent with the order of exchange being $O_B > O_T >$ NbOH $\gg O_C$. The exchange rate of the O_T and NbOH increases with decreasing pH while the exchange rate of the O_B is minimally affected by pH, suggesting that protonation of O_T and NbOH sites is involved in pH-controlled decomposition of $[Nb_6O_{19}]^{8-}$. These studies also show that the NbOH species exist in solution for a wide range of neutral to basic pH values (pH ≈ 7−11.0), with no significant degree of deprotonation observed. Comparison of solid-state and solution ^{17}O NMR revealed that the proton becomes more strongly bound to the bridging oxygen in solution and may help stabilize this highly charged anionic cluster by decreasing the overall charge. NMR investigations of diprototic hexaniobates, as well as solution behavior of the acid-stable hexamolybdate and hexatungstate, are in progress. This and ongoing studies will provide fundamental information into the differences between the stability and reactivity of base-stable polyoxoniobates and acid-stable polyoxotungstates and polyoxomolybdates.

Acknowledgment. Sandia is a multiprogram laboratory operated by Sandia Corporation, a Lockheed Martin Company, for the United States Department of Energy's National Nuclear Security Administration under Contract DE-AC04-94AL85000. We would also like to acknowledge the Sandia National Laboratories LDRD support of this research.

Supporting Information Available: Additional experimental results (PDF). This material is available free of charge via the Internet at http://pubs.acs.org.

JA0398159